



An optimized hybrid nanostructure for tunable radiation and filter characteristics in optical circuits

Vinay Kanungo¹ · Rukhsar Zafar² · Praveen K. Jain² · Vijay Janyani³

Received: 13 July 2023 / Accepted: 12 October 2023
© The Author(s), under exclusive licence to The Optical Society of India 2023

Abstract A hybrid nanostructure using gold nanoparticles encapsulated in a dielectric shell has been proposed. The proposed nanostructure offers radiation and filtering characteristics in visible wavelength range. First, the design has been optimized then two variations of the optimized design have been analyzed. Dielectric shell index values are kept less than 2 to keep the electric and magnetic scattering efficiencies under control. First design is the array of structure with constant shell index and varying shell surrounding conditions which offers narrowband filtering in visible spectrum. In this design, both the operational filter bandwidth and the radiation wavelength red shifts with increment in shell index values. Design with shell index 1.5 offers a 3-dB filter bandwidth of 87 nm which increases to 155 nm for shell index 1.95. Contrary to filtering, radiation resonance remains approximately constant with change in 3 dB radiation spectrum. The shell surrounding index is also critical in deciding the filter bandwidth as the offered filter bandwidth increases significantly with the surrounding index values greater than 1.3. Variation in the number of array elements causes no change in the power extinction and radiation characteristics, although it affects the far field radiation pattern. Array with larger number produces more elliptical radiation pattern. Further, keeping the surrounding index

constant and selecting different shell indices in the design offer wider 3-dB filter bandwidths and wideband radiation characteristics, and this forms the second proposed design. A wide 3-dB filtration band of 210 nm covering filtering bands offered by all the individual elements was achieved. Similarly, radiation pattern observes a wider spectrum covering spectrums of all the array elements. Analyzing the losses offered by dielectric shell, less than 20% of normalized shell loss are observed at 0.52 μm with lowest shell index, whereas it increases to more than 90% of the normalized loss values with highest index contrast at around 0.41 μm , which is sufficiently apart from the power extinction range of gold nanoparticle. All the simulations have been carried out using finite difference time domain method (FDTD).

Keywords Gold Particle array · Power extinction · FDTD · Far field pattern

Introduction

Conventional optics explains the radiation of wave fronts through lenses, mirrors, and diffractive instruments. The manipulation of photons at sub-wavelength scale cannot be achieved with conventional optics. This is the foundation of application of surface Plasmon effects to explore new possibilities in optical instrumentation which can go beyond conventional optics. In 1928, Edward Synge managed to break the diffraction limit by identifying the properties of colloidal gold particle in order to radiate the localized field [1] [2]. In 1995, John Wessel concluded that the gold nanoparticle can work as an optical antenna [3]. This was for the first time a nanoparticle was seen as a device to transfer information at such nanoscale level. Later on, optical antennas become a prominent tool for near-field microscopy and spectroscopy

✉ Rukhsar Zafar
rukhsarzafar1987@gmail.com

¹ Department of Computer Science and Engineering, Swami Keshvanand Institute of Technology, Management & Gramothan, Jaipur, India

² Department of Electronics and Communication Engineering, Swami Keshvanand Institute of Technology, Management and Gramothan, Jaipur, India

³ Department of Electronics and Communication Engineering, Malviya National Institute of Technology, Jaipur, India

[4], and were explored in various applications such as on the tip of atomic force microscopes [5] aperture-based near-field detectors [6, 7]. Recently the term optical antenna has gained lot of attention due to its capability of transforming the information from near field to far field effectively [8]. Optical antenna possesses capabilities of radio antennas, and offers the antenna characteristics in optical domain [8]. Phenomenon of surface Plasmon is unique and a key feature of optical antenna, making optical antennas applicable over a wide spectrum of applications including optical detection, biological sensing, optical sources, data storage, etc. [9–11]. Antennas can be designed to control the radiation effectively in microwave or radio frequency range but extension of radio antennas to the optical domain is not linear in nature [12]. Optical antennas have extensively been studied and experimentally tested through various well established geometries in RF domain such as dipole, Yagi-uda, bow-tie, etc. [12–15]. Recently an optical Yagi-Uda antenna has been fabricated for optical on chip communication as a light source (radiating element) [16]. This shows an analogical relation between the radio wave antenna and optical antenna, consequently providing directions for future development. In another work, Park et al. [17] presented the possibilities of metallic nanoslots to be used as optical antenna in integrated optical and photonic devices. They have also used the RF analogy to develop nanoslot Yagi-Uda antenna. In addition to the geometry resemblance with RF counterpart, optical antennas have also been tested for their near field (generated by a quantum dot or fluorescence emitter) to far field transmission characteristics which give them the title of antenna. In order to establish a theoretical background for the optical antenna operations, the extensive research carried out in RF domain can be utilized. This includes the modeling of far field radiation pattern, side lobes, antenna excitation, directivity, relation between wavelength and optical antenna structures. Although, both light and radio waves are defined by the Maxwell equations but still direct mapping of the theoretical concepts from RF to optical domain is not possible. Metal behaves differently in RF and optical domain due to underlying physics. In optical domain, antennas are dominated by polarization and displacement effect and this changes the physics behind the antenna operation from that of in RF domain. In optical domain, quantum theory of physics explains the light matter interaction, and this has theoretically been discussed in literature extensively [18–20].

Underlying physics

Surface Plasmon generation has been studied under the effect of light matter interaction, specifically when matter is of nanoscale dimension. The underlying physics explaining the results of energy interaction with nanoparticle get

transformed completely from that of bulk particle. A particle with dimension lying between 1 and 100 nm can be considered as nanoparticle. The incident energy trapped at the interface of two materials having positive (dielectric materials) and negative (metals) refractive index values is referred as surface plasmons and the trapped energy may be either of propagating nature or localized depending upon the size and shape of nanomaterial used. Selection of the type, size and shape of nanomaterial, excitation wavelength, and surrounding environment is determined by the area of application such as for applications in visible spectrum, Gold and silver nanoparticles are preferred metal due to their energy band gap lying in the visible spectrum [21]. Generation of surface plasmon require certain excitation conditions to be met and depending upon the fact various conditions for Surface Plasmon generation have been discussed in literature [22]. Here, it is to be noted that localized surface plasmons can be generated without matching the excitation conditions unlike their propagating counterpart. Drude model explains the dielectric behavior of metals over a wide wavelength range in optical domain. Although, due to interband transitions, the model starts to deviate from the actual response at higher side of the spectrum. This deviation of Drude's model is handled by incorporating an additional dielectric constant in the Drude's dielectric function giving the modified expression for noble metals [22].

In the proposed work, a nanostructure supporting localized Surface Plasmon generation has been proposed in view of its application as optical antenna and filter. The gold metal nanoparticles have been analyzed and simulation results have been obtained in view of the application of nanoparticle as nanoradiator and filters. It is clear from the above discussion that nanoparticles can effectively provide power extinction over a finite wavelength range. By varying the surrounding index of the particle, it is possible to achieve power extinction at different wavelengths. Different nanomaterial types with different shapes have been analyzed for application ranging from bioimaging [23], solar cells [24] to optical trapping [25]. In addition, arrays of such nanoparticles have also been explored for combined effect in applications such as optical antenna array, self-similar optical structures for enhanced SERS effect [26]. In this paper, a novel metal nanoparticle array design has been proposed for achieving antenna and filter operational characteristics to be applicable in optical circuits. The design makes use of nanoparticle optical characteristic variation in an array of nanoparticle collectively showing the integrated responses of all the array particles to have filtering and radiation properties over a certain wavelength range. Here, it is ensured that there should have no mutual coupling between the particle responses and particles retain their individual behavior. Although, the array produces results collectively but the

individual behavior of the elements can be kept intact by selecting proper inter-element separation. In the proposed design, dielectric shells containing the nanoparticles have been optimized for inter-particle separation and placed 3 times the shell radius apart from each other. The variation in responses of nanoparticles is achieved through varying the dielectric conditions for each nanoparticle within the array. Each particle in the array observes different surrounding conditions and collectively the array is offering desired extinction wavelength range of incident power.

Gold has been the preferred choice for a wide range of sensing and imaging applications due to high optical efficiency, chemical inertness, biocompatibility, relatively easy surface functionalization and bioconjugation, and highly nonlinear characteristics [27]. Gold nanoparticle with varying conditions (size, surrounding index) can offer Surface Plasmon generation over visible to near infrared (NIR) wavelength range [21]. Further, the operating wavelength range can be controlled by proper selection of refractive indices, number of array elements, and aspect ratio of the nanoparticle [21]. The unique design of Gold nanoparticles embed in dielectric shell has been studied for filter and antenna applications over the above-mentioned wavelength range of interest. The proposed structure is numerically analyzed using finite difference time domain (FDTD) method.

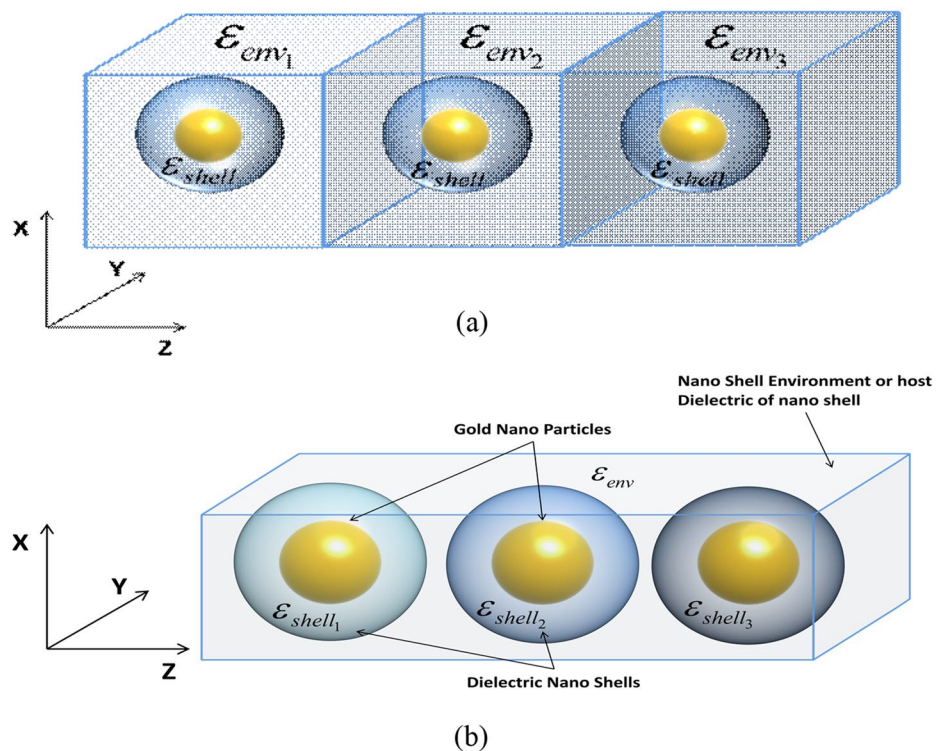
Proposed structure

Figure 1 shows the two proposed array designs in which the gold nanoparticle is embedded in a dielectric nanoshell. The diameter of gold nanoparticle is 100 nm and that of the dielectric nanoshell is 240 nm. In this paper, the proposed design obtained after optimizing the size of dielectric shell has been analyzed for its application in optical antenna and filter design. The analysis has been done based on the following two possibilities through which the aforementioned design objectives can be achieved:

- Variation in the surrounding index of the dielectric shell
- Variation in the index of dielectric shell while keeping the surrounding index constant

The above-mentioned two possibilities of index variation give rise to the two different types of geometrical arrangements of the proposed design. Figure 1a is showing the first type of arrangement where all the dielectric shells are of same material and only the surrounding or host material of the dielectric shell is changing. The second arrangement is depicted in Fig. 1b where different surrounding index conditions for gold nanoparticles in the array has been achieved through dielectric shells of different refractive index ($\epsilon_{shell_1}, \epsilon_{shell_2}, \epsilon_{shell_3}$). Further, the array of dielectric shells containing gold nanoparticle has been placed in an environment or a host material (ϵ_{env}). Here, ϵ_{shell} and ϵ_{env} are the dielectric constant of the shell and its environment,

Fig. 1 Proposed array of dielectric nanoshells of identical refractive index in different dielectric host environment (a); Proposed array (3 elements) of dielectric nanoshells of different refractive index containing gold nanoparticle inside, the array is placed in a dielectric host environment of permittivity ϵ_{env} (b)



respectively. The environment is constant throughout the array in case of the second type of array design, whereas it is varied to achieve the filter and antenna operations in case of the first type of design while keeping the shell index constant throughout the array. The arrangement with variable shell index offers a wider filtration bandwidth, and a radiation pattern with wider main beam characteristics in comparison to the design with variable shell environment index.

Nanoparticles in the arrangement are studied for their individual responses and hence mutual coupling between the particles is avoided by keeping the element separation distance 3 times the shell radius. The inter-element separation distance has been decided on the fact that the mutual coupling between the particles scales with d^{-3} [22]. Power losses due to dielectric shell have also been investigated in order to observe the existence of any interference with the surface Plasmon resonance wavelength. In Fig. 1, different shades are representing the different indices of dielectric material. In order to achieve maximum illumination from external light source ϵ_{env} is always kept less than or equal to ϵ_{shell} . In this paper, dielectric shell index ($N_{shell} = \sqrt{\epsilon_{shell}}$), and surrounding host or environment index ($N_{env} = \sqrt{\epsilon_{env}}$) have been used for analysis of the design in visible to near infrared wavelength range.

Theoretical Background

The nanosized metal particles when operated in the optical band, it attains dielectric character and the dielectric constant of metal with interband transition correction is defined by the Drude theory as explained in Eq. 1 [22]

$$\epsilon(\omega) = \epsilon_{\infty} - \frac{\omega_p^2}{\omega^2 + i\nu\omega} \tag{1}$$

where ϵ_{∞} varies in the range 1 to 10. Drude model explains the behavior of metal in the optical frequency range till the interband transitions in metal occurs. Interband transitions are the resultant effect of absorption of the incident photon ultimately affecting the generation of surface plasmons. For Gold, these transition starts occurring at the boundary of near infrared and visible spectrum. To model these interband transitions, the expression of dielectric function given by the Drude model was modified by adding a Lorentz-oscillator term $\frac{A_i\omega_i^2}{\omega_i^2 - \omega^2 - i\nu\omega}$ and the dielectric function is now given by [22]

$$\epsilon(\omega) = \epsilon_{\infty} - \frac{\omega_p^2}{\omega^2 + i\nu\omega} + \sum \frac{A_i\omega_i^2}{\omega_i^2 - \omega^2 - i\nu\omega} \tag{2}$$

The definition of metal dielectric constant is further utilized in calculation of the amount of scattering and absorption by the nanoparticles. Mie theory relates the incident power to the

scattered and absorbed power in terms of geometrical quantities known as extinction cross section and scattering cross section. From Mie theory the scattering and absorption cross section are given by [8, 24]

$$\sigma_{ext} = \frac{2\pi}{k^2} Re(a_n + b_n) \tag{3}$$

$$\sigma_{sca} = \frac{2\pi}{k^2} \sum_{n=1}^{\infty} (2n + 1) (|a_n|^2 + |b_n|^2) \tag{4}$$

$$\sigma_{abs} = \sigma_{ext} - \sigma_{sca} \tag{5}$$

The coefficients a_n and b_n are defined as [8]

$$a_n = \frac{m\psi_n(mx)\psi'_n(x) - \psi_n(x)\psi'_n(mx)}{m\psi_n(mx)\xi'_n(x) - \xi_n(x)\psi'_n(mx)} \tag{6}$$

$$b_n = \frac{\psi_n(mx)\psi'_n(x) - m\psi_n(x)\psi'_n(mx)}{\psi_n(mx)\xi'_n(x) - m\xi_n(x)\psi'_n(mx)} \tag{7}$$

Where ψ and ξ are Ricatti-Bessel functions of order n , k is wavenumber, $x = kR$ is size parameter (R is radius of metal particle) and $m = \sqrt{\frac{\epsilon_p}{\epsilon_m}}$ is the square root of the ratio of dielectric functions of particle and of the medium. For very small metal particles (smaller than wavelength), the expressions denoted by Eqs. (3-4) can further be simplified by applying the Rayleigh limit ($mx \ll 1$, where $x = kR$). The simplified expressions for the cross sections are given by [8] [23].

$$\sigma_{abs} \approx \sigma_{ext} = kIm(\alpha) = 4\pi kR^3 Im\left(\frac{\epsilon_p - \epsilon_m}{\epsilon_p + 2\epsilon_m}\right) \tag{8}$$

$$\sigma_{sca} = \frac{k^4}{6\pi} |\alpha|^2 Im(\alpha) = 8\pi k^4 R^6 \left|\frac{\epsilon_p - \epsilon_m}{\epsilon_p + 2\epsilon_m}\right|^2 \tag{9}$$

Where α is the polarizability of the particle which is defined as [8] [23].

$$\alpha = 4\pi R^3 \frac{\epsilon_p - \epsilon_m}{\epsilon_p + 2\epsilon_m} \tag{10}$$

ϵ_p and ϵ_m are the dielectric constants of the particle and the medium, respectively. Equations (8) and (9) are also applicable for nanodielectric particles satisfying the Rayleigh limit [22]. At Surface Plasmon resonance condition, σ_{abs} and σ_{sca} become greater than the physical cross section of nanoparticle. The resonance condition is given by the Frohlich criteria [8] [23].

$$Re[\epsilon(\omega)] = -2\epsilon_m \tag{11}$$

From Eqs. (8) and (9), a clear dependency on particle size can be seen. Scattering increases with 6th power of particle size whereas absorption increases with 3rd power of the particle size. Consequently, for smaller particles, an absorption cross section will be greater than the scattering cross-section and therefore absorption-based analysis of very small particles is preferable than scattering-based analysis [22]. Although, the power extinction analysis will be applicable for a wide range of particle dimension as it includes both scattered and absorbed power. In addition, Eq. 12 gives an idea about how change in surrounding index can lead to shift in the resonating condition. As Eqs. (8) and (9) from Mie theory are applicable for both dielectric and metal nanoparticles with dependencies on particle size [22], it is clear that the equations from (8) to (11) can be used to explain the power extinction characteristics of the proposed design. Hence, the FDTD method with Drude dispersion model has been used to simulate the proposed design and the results have been obtained in view of its application for antenna and filter design.

Result and discussion

The performance of the proposed structure is analyzed for power extinction and scattering spectrum. At first, shell radius optimization through the analysis of power extinction and scattering responses observed using FDTD method has been performed. The objective of shell radius optimization is to achieve response closer to the individual metal nanoparticle response (isolation from dielectric shell absorption peaks) and obtaining mutual isolation when placed in an array of such particles. Further, the optimized design has been investigated for filter and antenna application by varying the index contrast between shell dielectric index and host material index.

Figures 2 and 3 are showing the effect of varying the shell size on power extinction and corresponding radiated power or scattered power, respectively. The inter-band transitions (d-d transitions) corresponding to localized surface plasmon generation for noble metals lies in the visible to near infrared wavelength range. Hence the proposed design has been investigated within the above-mentioned wavelength range. Results in Figs. 2 and 3 have the following design considerations: the shell index (N_{shell}) is 1.5, host dielectric is air, and diameter of nanoparticle is 100 nm. In case of without

Fig. 2 Power extinction with varying shell radius

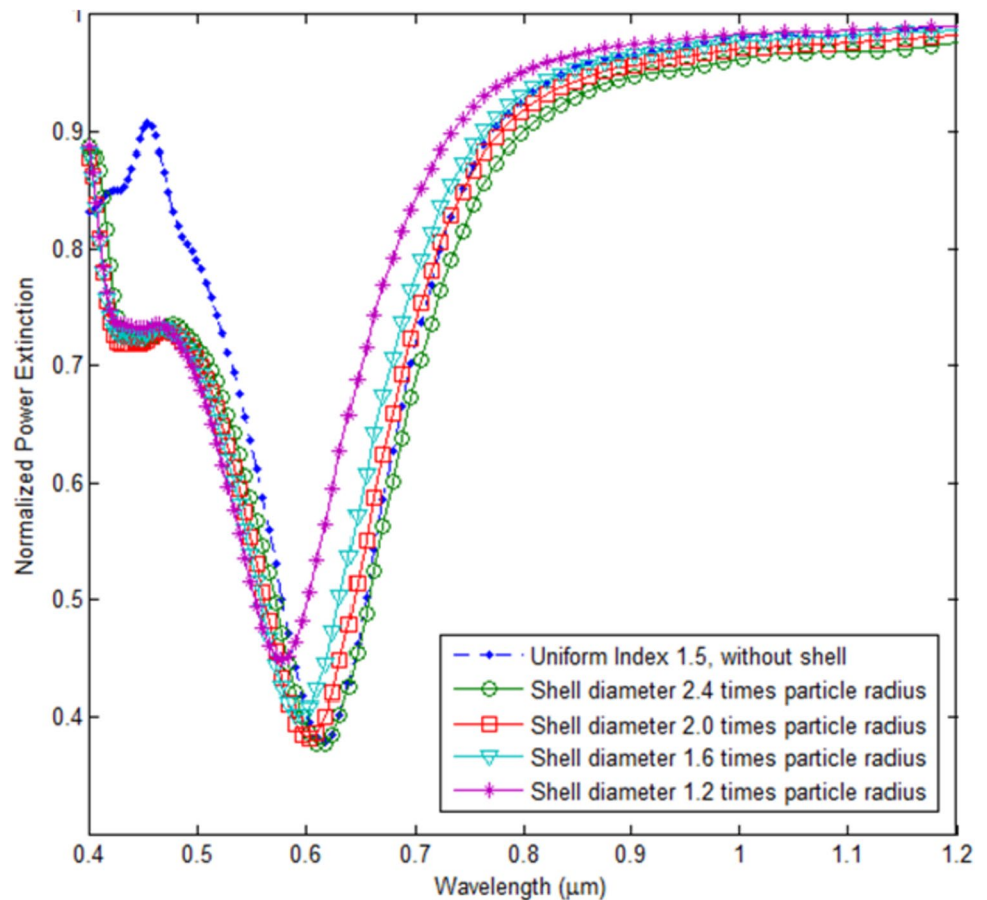
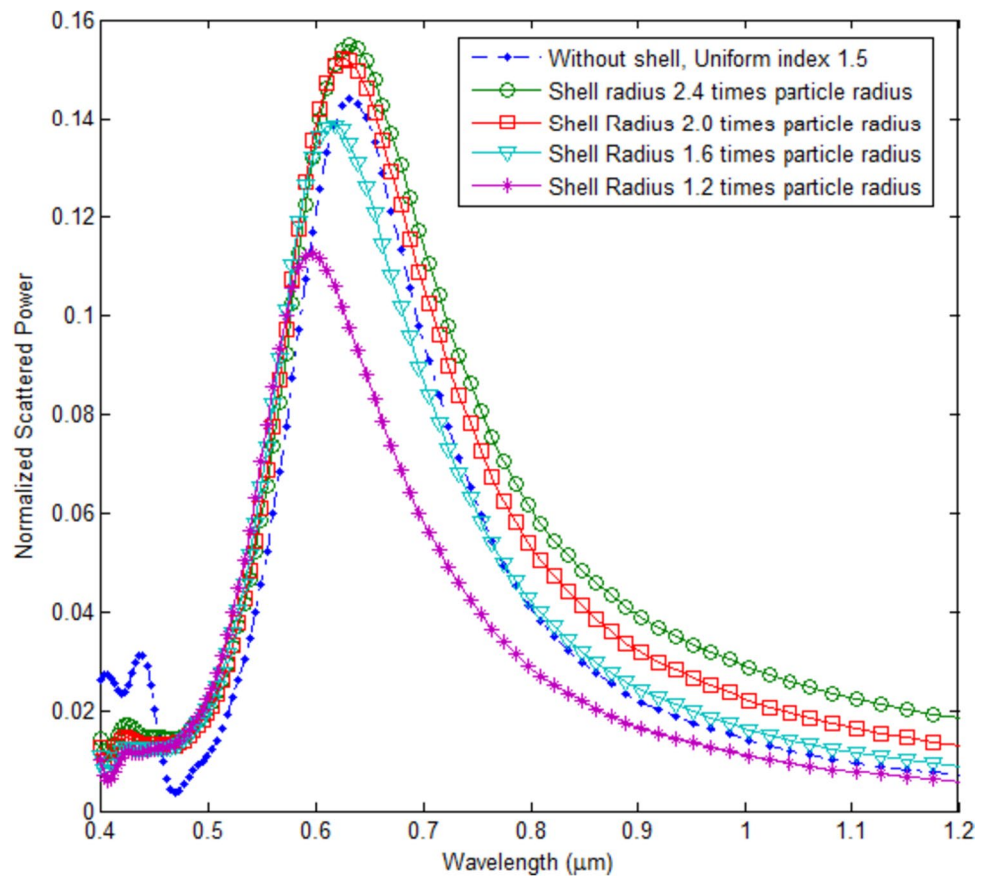


Fig. 3 Power scattered with varying shell radius



shell analysis, shell environment index becomes equal to the dielectric shell index. Consequently, the gold nanoparticle is uniformly surrounded by a constant refractive index and for the above case it is 1.5 ($N_{shell} = N_{env} = 1.5$). The without shell responses (uniform surrounding) in Figs. 2 and 3 are indicated with blue dotted lines. When shell size is increased, it tends to increase the effective refractive index around the gold nanoparticle and excitation responses shifted toward higher wavelength side of the spectrum (red shift). These responses are quite obvious and are in agreement with the analysis carried out in [21]. Increment in the scattered power amplitude is also in agreement with results obtained in [21] as with increment in the surrounding index, scattering power also increases. Figure 2 shows the collective (dielectric and metal) power extinction characteristics, and with shell radius 2.4 times the gold nanoparticle, the extinction response is at minimum separation from that of uniform surrounding index response. Figure 3 shows the scattered power characteristics; dielectric shell with 2.4 times the gold nanoparticle offers the same resonance wavelength as obtained with uniform surrounding index, although slight increment in amplitude is observed. These observations can be explained on the

fact that the proposed design is a combination of a larger dielectric shell and a smaller gold nanoparticle. Now the response of the proposed unique design can be explained with the scattering and absorption efficiencies offered by the two integrated particles (metal and dielectric). Following section explains the results in Fig. 2 in view of Mie theory and also establishes the ground for understanding the other results reported in this paper.

As mentioned previously in the theoretical background through Eqs. (8) and (9), excitation characteristics of smaller particles are well explained by absorption cross section whereas for larger particles, the responses are dominated by scattering cross section. In case of lossless and non-magnetic materials, the scattering efficiencies are determined by the dielectric permittivity ϵ and size parameters $q = 2\pi r/\lambda$ of the material [28]. Dielectric material used for shell (ϵ_2) in the proposed design varies from $N_{shell} = 1.5$ to 1.95. The considered range of dielectric material includes some low index to high index glasses [28]. These glasses are not completely lossless but offer very less absorption losses in the visible to infrared wavelength range in comparison to the metals.

Hence in the proposed design, the index contrast $\left(\frac{N_{shell}}{N_{env}}\right)$ defined as the refractive index ratio of dielectric shell to the shell environment and particle size determine the scattering efficiency which dominates the dielectric nanoparticle response. Gold nanoparticle in the proposed design is the major contributor toward the absorption loss offered by the design in the wavelength range of interest.

The excitation responses offered by the dielectric and gold nanoparticles are significantly different in terms of electric and magnetic field resonances [29, 30]. Effect of these field resonances will be discussed later in the section in view of the design excitation responses. Let us now consider Fig. 2, the index contrast and gold nanoparticle size is kept constant while varying the size of dielectric shell. Now, in order to understand the excitation behavior of the proposed design in Fig. 2 let us consider the following equation in view of Mie theory

$$P_{ext} = P_{scattered} + P_{absorption} \quad (12)$$

where P_{ext} , $P_{scattered}$, and $P_{absorption}$ are the total power extinguished, power scattered, and power absorbed, respectively, by a nanoparticle of radius r . Here we have assumed that absorption loss is an abstraction of all other possible losses (such as heat loss) associated with nanoparticle. These power values are directly depending upon the cross section values obtained from Eqs. (9) and (10) and are function of particle size. Particles with dimensions much smaller than the wavelength of applied excitation field ($r \ll \lambda$ or $q \ll 1$) can be analyzed with quasi static approximation and metal particles with such dimensions produce localized surface plasmon resonances containing the electric field responses only while offering no magnetic field responses. Very small metal nanoparticle offers electric dipole resonance whereas increment in size may produce higher order modes containing electric quadrupole. On the other end, dielectric nanoparticles can offer both magnetic and electric field resonances of comparable strengths. These fields exist in terms of dipole, quadrupole, and other higher multi-poles [22, 29]. The scattering response of high index dielectric nanoparticles ($N_{shell} \geq 2$) with sizes ranging from 100 to 300 nm contains four major resonance modes: electric dipole, magnetic dipole, magnetic quadrupole, and electric quadrupole. With increment in particle size, the four major modes start appearing prominently and out of them, the dipole modes are the dominating ones. In addition, the size increment also causes red shift in the resonance wavelength corresponding to the electric and magnetic dipole modes across the complete visible spectrum along with the generation of new higher order modes [29, 30]. Moreover, at magnetic resonance wavelength, the

contribution of magnetic dipole mode in the scattering response of a high index dielectric nanoparticle exceeds all other existing multi-pole modes by order of magnitude. This occurs when wavelength inside the nanodielectric become comparable to the particle dimensions, i.e., $\frac{\lambda}{N_{shell}} \approx 2r$, where λ is the resonance wavelength.

It is to be noted here that scattering efficiencies associated with all the discussed electric and magnetic modes are significant for high index ($N_{shell} \geq 2$) dielectric nanoparticle and are directly proportional to n . In the proposed design, gold nanoparticle embedded in dielectric shell have been analyzed and simulated for their application in optical filter and antenna application. The objective of dielectric shell is to provide different surrounding conditions around gold nanoparticle for surface plasmon generation so that when used in array can offer required operation in the wavelength range of interest. So low index values ($N_{shell} < 2$) of dielectric shell are chosen to have high transparency, minimum absorption losses and to have lower intensities of electric and magnetic resonance modes. With $N_{shell} < 2$, and a diameter of 240 nm, the proposed design quite satisfy the mentioned objectives and offer weak electric and magnetic modes (dipole, quadrupole, and higher order modes) to have minimum interference with gold nanoparticle surface plasmon resonance modes.

Now, with the given explanation, we can easily express these power values in Eq. (12) as a function of particle radius (r) and the particle dielectric constant ϵ_p . Hence, re-writing Eq. (12) as

$$P_{ext}(r, \epsilon_p) = P_{scattered}(r, \epsilon_p) + P_{absorption}(r, \epsilon_p) \quad (13)$$

For metal nanoparticle $\epsilon_p < 0$;

for dielectric nanoparticle $\epsilon_p > 0$

From Fig. 2, since the gold nanoparticle size is constant, the increment in scattered power is due to the increasing effective refractive index as a result of increment in dielectric shell size, as show in Fig. 2. Scattering response or normalized radiated power of gold nanoparticle is also influenced by the scattered power of dielectric shell at lower index contrast values through the electric dipole mode coupling. Initially with increment in index contrast, significant contribution from the dielectric shell scattered power is observed at gold nanoparticle scattering resonance wavelength due to electric dipole mode coupling. Further increment in index contrast causes generation of higher order modes for both electric and magnetic resonances. This saturates the contribution of dielectric shell at gold nanoparticle resonance wavelength while increasing the dielectric shell power extinction losses

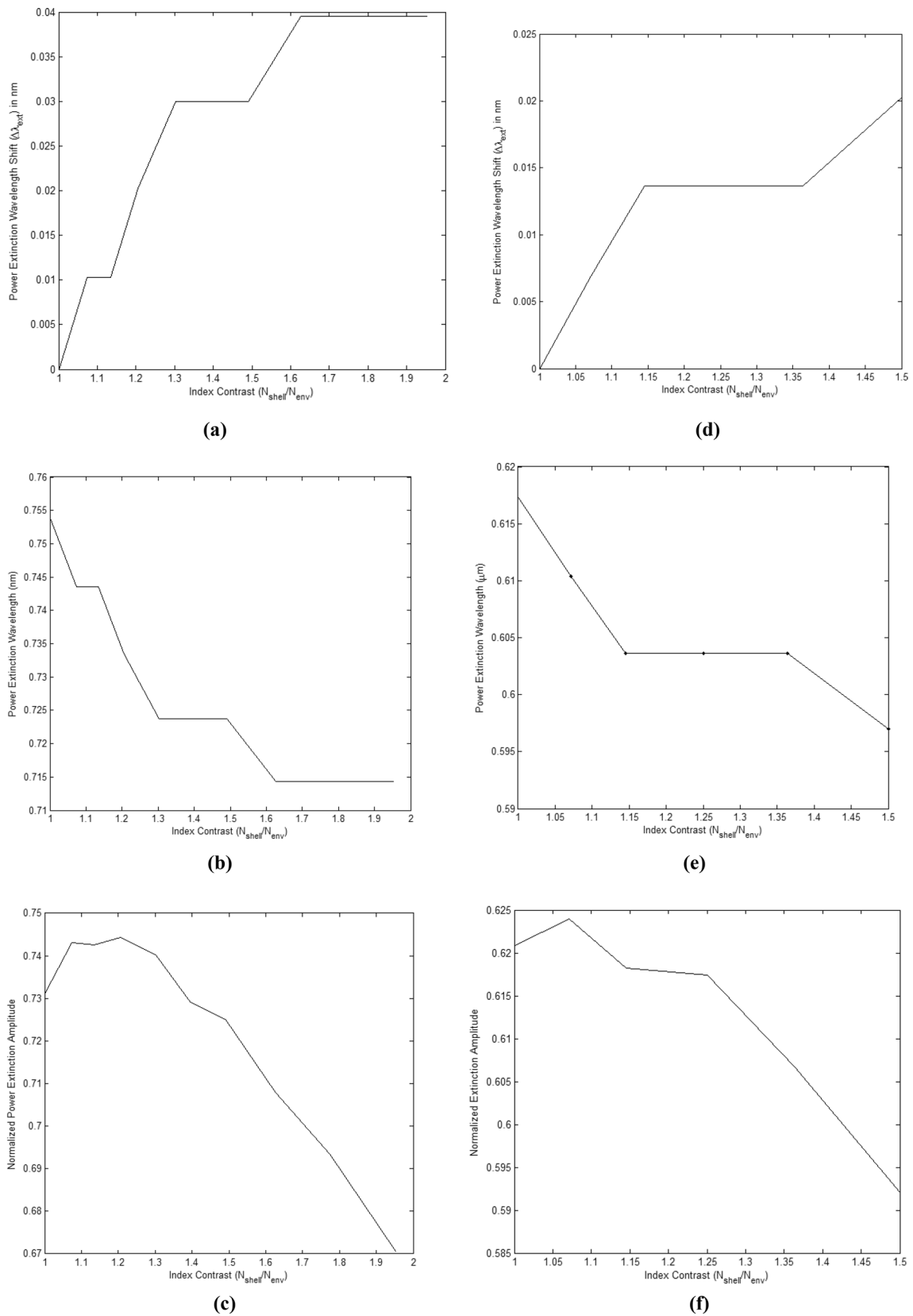


Fig. 4 Power extinction wavelength shift (difference from original wavelength) (a); magnitude of shift in extinction wavelength (b); change in extinguished power (c) with index contrast change for shell index = 1.95. Same in order for shell index 1.5 are depicted by (d), (e), and (f)

dominated by magnetic dipole mode resonance at lower side of the excitation wavelength range, discussed later in this paper. In Fig. 2, the index contrast takes the value 1 for uniform surrounding ($N_{shell} = N_{env} = 1.5$), and 1.5 for all the remaining cases where $N_{shell} = 1.5$ and $N_{env} = 1$. For index contrast 1.5, constructive scattering power interference from the dielectric shell at the scattered power resonance wavelength of gold nanoparticle is observed. Hence, in Eq. (13), the scattered power component is a resultant of dielectric shell and gold nanoparticle scattered power responses through electric dipole mode coupling. From Fig. 2, we can clearly see that the scattered power response of gold nanoparticle exceeds the response obtained in case of uniform surrounding index ($N_{shell} = N_{env} = 1.5$, shown with blue dotted line) due to the dipole mode coupling from dielectric shell. Again from Eq. (14), since the total power extinction response has a dependency on scattered and absorbed power responses, power extinction response in Fig. 2 cannot be explained without considering the absorption characteristics of both the particles. Total power extinction of the proposed design should increase as a result of increased scattered power of gold nanoparticle due to the coupling of electric resonances of metal and dielectric, as mentioned previously. From Fig. 2a, the extinction power response of gold nanoparticle increases initially with dielectric shell size due to the increment in the scattered power response but at the same time absorption losses associated with gold nanoparticle starts decreasing. Two factors working simultaneously against each other cause power extinction response to deviate from the scattered power response. As for the gold nanoparticle (where $r \ll \lambda$), excitation response is dominated by the absorption cross-section, it is quite clear from Eq. (13) that the total power extinction for gold nanoparticle is a resultant of the collective (metal nanoparticle and dielectric shell) scattered power response and the dominating absorption power response restricting the total power extinction response to increase further. Hence further increment in shell size (greater than 2.4 times the nanoparticle) causes reduction in the total power extinction offered by the gold nanoparticle and this trade-off result in an optimized value of dielectric shell that is 2.4 times the nanoparticle where the response is at minimum separation from that of uniform surrounding index.

As mentioned previously that the shell index contrast variation also affects the total power extinction offered by the proposed design, so the optimized design discussed above has been investigated for different shell index contrast. Figure 4 depicts the changes in extinction resonance wavelength of gold nanoparticle embedded in dielectric shell with variation in index contrast along with the offered power extinction amplitude. Here two shell index value designs that is 1.95 and 1.5 have been considered and the contrast is varied by varying the host index of dielectric

shell (see Fig. 1a). It is to be noted here that for both the design considerations, responses in view of the index contrast variations are quite similar. As can be seen from Fig. 4b and e, with rise in index contrast, blue shift in the gold nanoparticle resonance is observed due to the presence of dielectric shell. The collective (gold and dielectric shell) power extinction resonance shifts toward shorter wavelength in comparison to the gold nanoparticle resonance wavelength with increment in index contrast. This deviation is observed due to the fact that the net power extinction is resultant of the absorption loss (dominating for metal nanoparticles) from gold nanoparticle, and the dielectric shell scattering loss (dominating for dielectric nanoparticles) due to the electric and magnetic resonating modes offered in the gold nanoparticle resonance wavelength range (0.62–0.75 μm). A maximum of 40 nm shift (for shell index 1.95) in wavelength is observed for maximum index contrast and this phenomenon can be used to design narrowband optical filters in nano-integrated circuits. Figure 4a and d is showing the shift in resonating wavelength corresponding to the rise in index contrast for shell index of 1.95 and 1.5, respectively. Hence, an array of the proposed dielectric shell embedding gold nanoparticle can be formed in an environment of graded index profile to achieve the desired bandwidth of filter operation (shown in Fig. 4a and d).

Power extinction responses as a function of index contrast have been plotted in Fig. 4c and f for shell index 1.95 and 1.5, respectively. The reason for this extinction behavior of the proposed design in the gold nanoparticle resonance wavelength range was mentioned earlier in the section. At initial contrast values, the coupling between the electric dipole modes of the dielectric shell and gold nanoparticle brings slight increment in the curve (see Fig. 4c), where after it starts decreasing due to the generation of other higher order scattering modes (both electric and magnetic) of dielectric shell including the dominating magnetic dipole resonance. These scattering resonance modes of dielectric shell cause decrement in the overall power extinction offered by the design in the gold nanoparticle resonance wavelength regime (dominated by gold absorption cross-section). Losses associated with dielectric shell have been discussed in detail in the next section.

Figure 5 is showing the scattering wavelength and power variation with index contrast for shell index of 1.95. As mentioned previously in the discussion, coupling between the scattered electric dipole modes of dielectric and metal nanoparticles provides slight increment in the response for initial index contrast values. Further increment in index contrast causes generation of higher order electric and magnetic modes, although weak in strength due to lower index value of dielectric shell, causing the scattered power response to saturate and remain approximately constant. As

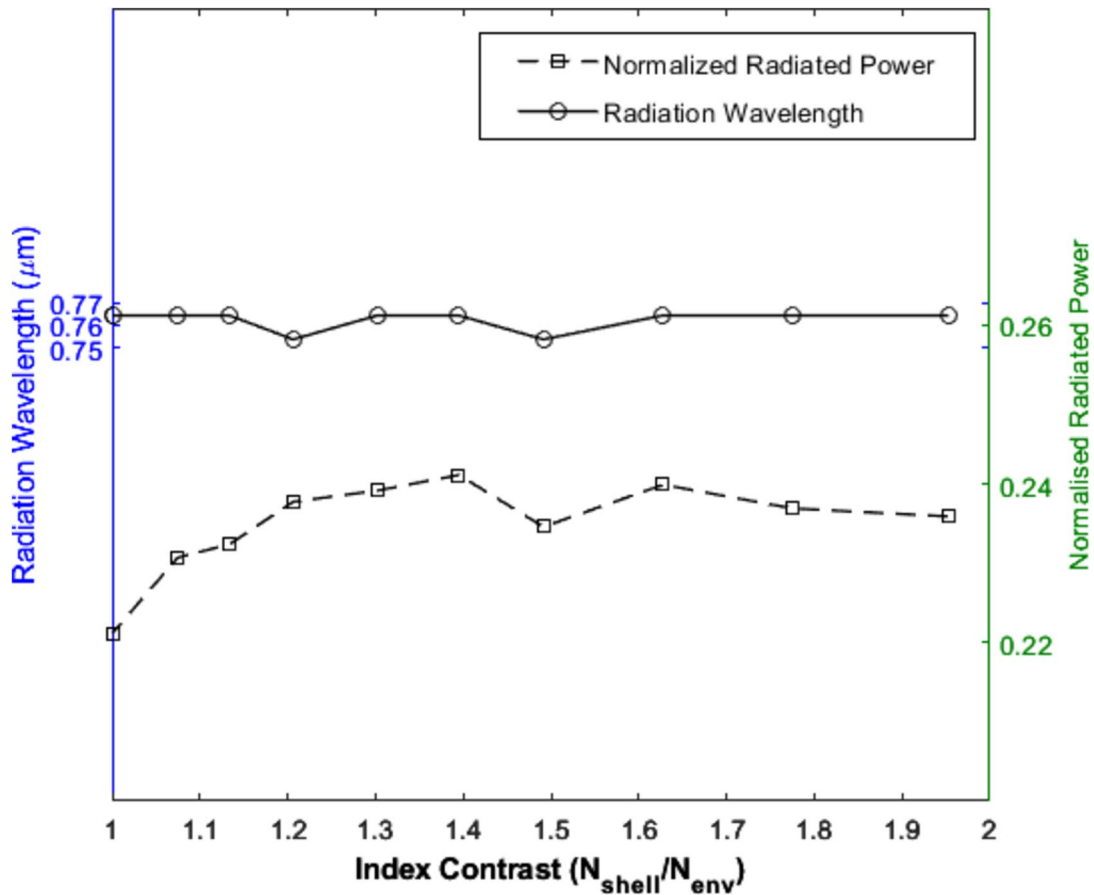


Fig. 5 Variation in radiation amplitude and wavelength with index contrast for shell index = 1.95

a consequence of the optimization of the proposed design in terms of dielectric shell radius (see Fig. 2), the scattered power resonance wavelength for gold nanoparticle remains approximately constant with index contrast variation (see Fig. 5). This is not the case for power extinction response as we have observed in Fig. 4, where shifting in the resonance wavelength was observed with index contrast variation. In power extinction response, changes in absorption losses associated with gold nanoparticle in view of the magnetic dipole mode, dominating the scattering losses associated with dielectric nanoshell plays the key role, as discussed previously. Since in the proposed design, dielectric shells with refractive index not exceeding a value 2 ($N_{shell} < 2$) have been considered, all the excited dielectric poles are weak in strength. When magnetic dipole resonance occurs, it provides major contribution to the scattering efficiency of dielectric nanoshell as it offers scattering efficiency order of magnitude higher than other multipoles [29]. In the next

section, losses associated with dielectric nanoshell have been discussed, specifically observing the scattering losses due to magnetic dipole resonance condition.

Dielectric shell losses

For dielectric nanoshell, now we understand that the power extinction behavior is explained through its scattering response. In this section, we are discussing the observed power extinction characteristic of dielectric shell depicted through Figs. 6 and 7. For dielectric particles both electric and magnetic type resonances are observed. But when the incoming light couples with the circular displacement currents of the electric field, it results in the resonant magnetic dipole response. It is interesting to note that the resonance wavelength of excited mode inside the particle is comparable to the particle diameter that is $\frac{\lambda}{N_{shell}} \approx 2r$. The proposed

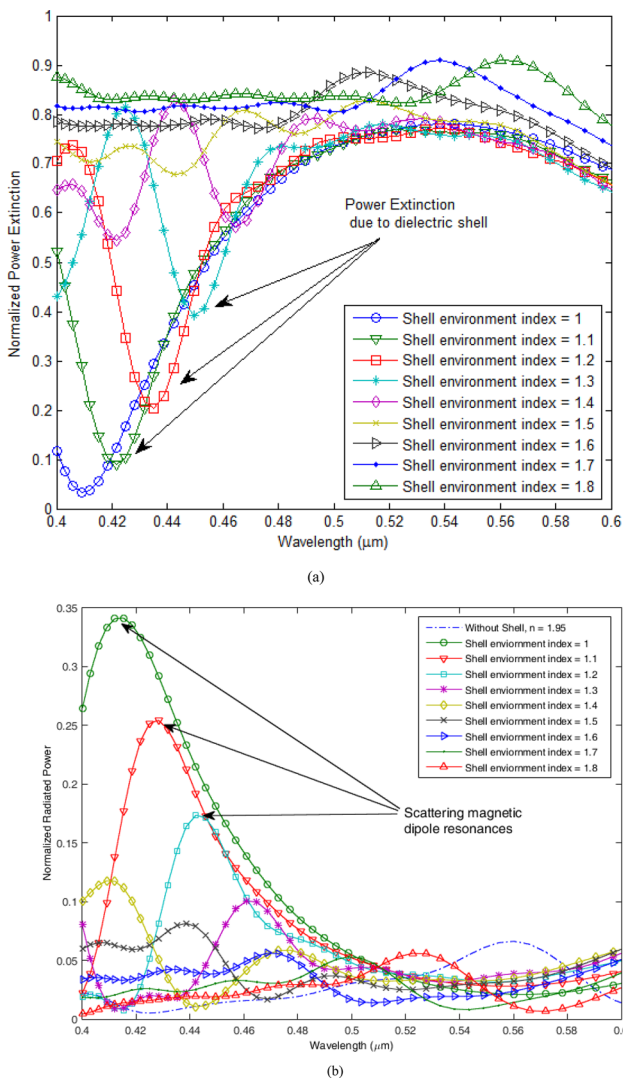


Fig. 6 Losses due to dielectric shell with varying host index, shell index = 1.95; Extinction loss (a); scattering loss (b)

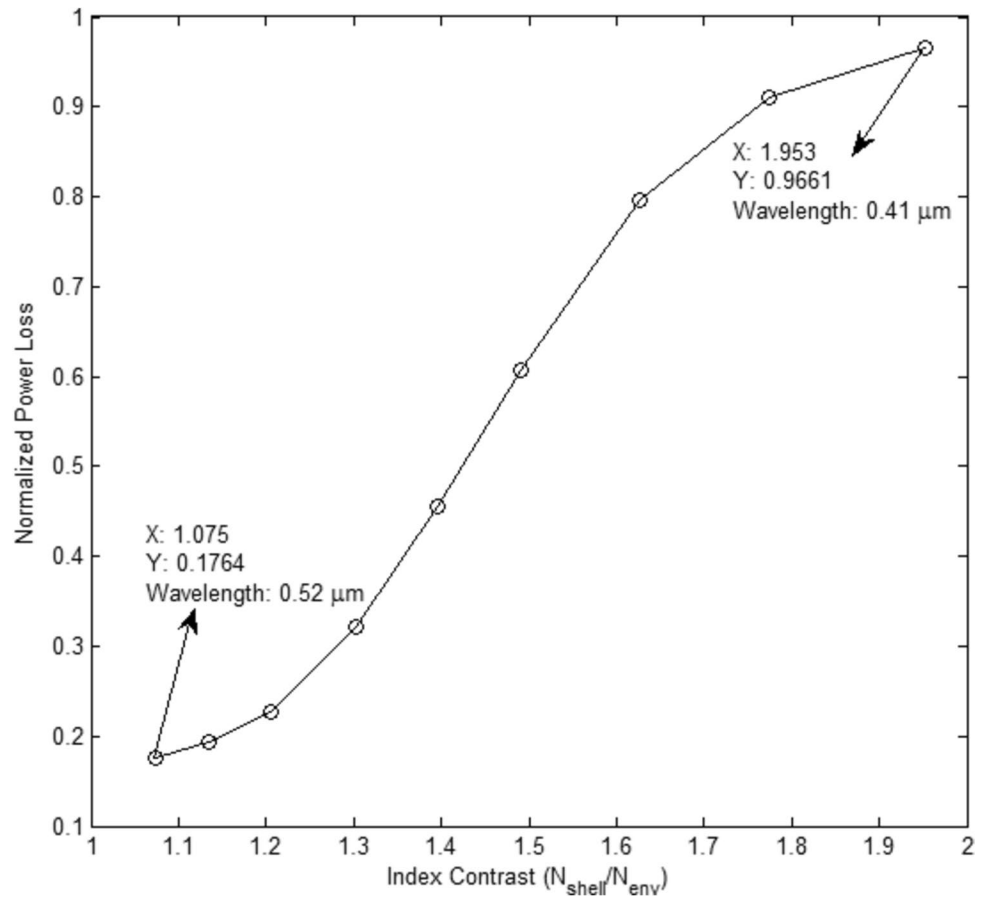
design has been investigated for the generation of magnetic dipole mode based on the aforementioned relation. In case the particle size is fixed, changing the refractive index of the material will lead to the change in resonance wavelength in order to keep the ratio $\frac{\lambda}{N_{shell}}$ approximately constant. However, here the case is slightly different as the dielectric shell index is constant ($N_{shell} = 1.95$) and variation in the refractive index of the particle surrounding is causing the magnetic dipole resonance wavelength to change. Results for net power extinction losses and scattering losses for the dielectric shell ($N_{shell} = 1.95$) are plotted in Fig. 6a and b, respectively. From Fig. 6b, scattering amplitude peaks corresponding to the magnetic dipole resonance are observed at lower

side of the spectrum. The strength and positions of the peaks varies with refractive index contrast in accordance with the behavior observed for gold nanoparticles [22] and can be explained through equations from (8) to (11) in this paper. The resonance peak becomes significantly weak in strength with index contrast falling below 1.4 as a consequence of reduced scattering losses by the dielectric shell. The wavelength range for the observed magnetic dipole resonances is 0.42 μm to 0.48 μm, which corresponds to a range of $\frac{\lambda}{N_{shell}}$ 0.21 μm to 0.24 μm. These values are of the order of dielectric shell diameter $D_{shell} = 0.24\mu\text{m}$, fulfilling the resonance conditions required for magnetic field excitation. Practically, dielectric shell design implementation can be done with a Niobophosphate high index glass (Ohara-SNPH-3), which offers refractive index values between 2.05 to 1.9 for visible to near infrared wavelength range [30]. The total power extinction offered by the dielectric shell is dominated by the scattering losses, particularly the magnetic dipole resonances observed at the beginning of visible spectrum (see Fig. 6a). As expected, the change in resonance wavelength and corresponding amplitude for extinction cross section is in agreement with the scattering losses (Fig. 6b) and hence has a significant dependency on index contrast variation. It is to be noted here that the resonance wavelengths for net power extinction are slightly shifted than that of scattering losses as the net power extinction includes losses due to refraction, reflection, and absorption by the dielectric shell. The change in power extinction characteristics of dielectric nanoshell as a function of index contrast in summarized in Fig. 7. It can be seen clearly that with increment in index contrast, extinction cross section of the dielectric shell increases with blue shift in the resonance wavelength. More than 96% of the transmitted power is lost for an index contrast of 1.95 at 0.41 μm, whereas it falls below 50% for an index contrast of 1.4 or less. Figure 7 shows a power loss spectrum of width around 0.1 μm(0.41μm – 0.52μm) with minimum and maximum values of power loss occurring at index contrast values close to 1 and 2, respectively.

Filter and antenna application of the proposed design

The proposed design with two different dielectric variation possibilities (Fig. 1) has been investigate for its antenna and filter application. This section presents the detailed discussion on the filtering and radiation characteristics of the designs obtained through finite difference time domain method of design modeling. In the first type of array, identical dielectric shells containing gold nanoparticle are placed in a graded index environment (variation in the dielectric

Fig. 7 Dielectric shell loss with index contrast; Highest loss occur at $0.41 \mu\text{m}$, starting of the visible spectrum and quickly end at $0.52 \mu\text{m}$. Losses for maximum index contrast variation occurs over a bandwidth of $0.1 \mu\text{m}$



shell host index) where due to the change in surrounding index, each element offers different resonance wavelength of power extinction, and collectively as an array offering a range of power extinction. Now at first, let us understand the behavior of the array with respect to the variation in different design parameters in order to establish the working of the design. In the first type of array, we have fixed shell index throughout the design but variable surrounding conditions. The design has been investigated for different values of shell index to observe the behavioral change and its operational differences. Figures from 8 to 10 are showing the power extinction (filtering) and radiation (scattering) characteristics for shell index values 1.5, 1.7, and 1.95, respectively, while varying the surrounding host index. From Fig. 8, for shell index 1.5, the power extinction is calculated with 3 dB bandwidth and it is observed over an 87 nm wide wavelength range starting from 563 to 650 nm. The peak to peak extinction resonance wavelength shift is observed from 597 to 617 nm. Figure 8b is showing the scattered power response for the surrounding index variation where the scattered power resonance (radiation wavelength) is

concentrated at single wavelength ($\lambda = 0.63 \mu\text{m}$) despite the variation in surrounding index (graded index variation of refraction) and this leads to its application as a narrow-band visible light radiator or optical antenna. Now when we increase the shell index value and analyze the design in similar way, the results are different in terms of offered 3-dB bandwidth and the wavelength range of operation (peak to peak resonance wavelength). Figure 9 shows the results for shell index 1.7; here the offered 3-dB bandwidth increases to 130 nm, whereas the operational wavelength range shifts toward higher side of the spectrum starting from 654 to 687 nm. Again from Fig. 10a, the 3-dB bandwidth for shell index 1.95 further increases to 155 nm along with red shifting of the operational spectral range from 714 to 754 nm. As expected, the red shift is also observed in the radiation characteristics of the design and in Fig. 10b, the radiation peak for shell index 1.95 is observed at $0.76 \mu\text{m}$, red shifted in comparison to that of shell index 1.5. Table 1 summarizes the results obtained for three different shell index materials for their filtering operation. These observations establish a clear dependency of the filter bandwidth and radiation

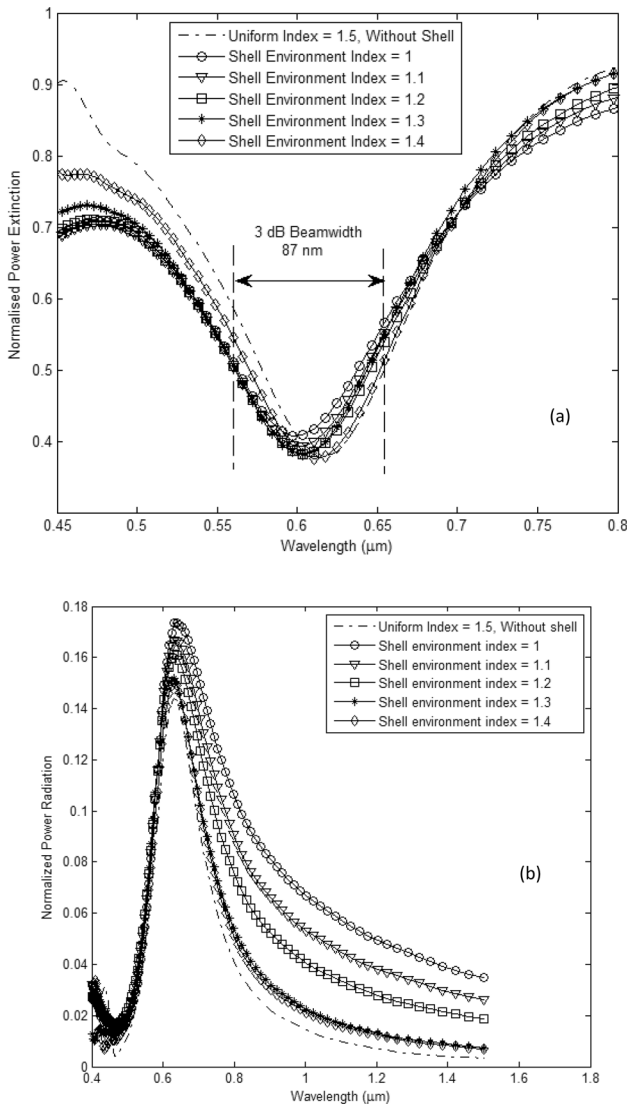


Fig. 8 Power Extinction (filter operation) (a) and radiation (b) curve for change in index contrast of a dielectric shell of index 1.5

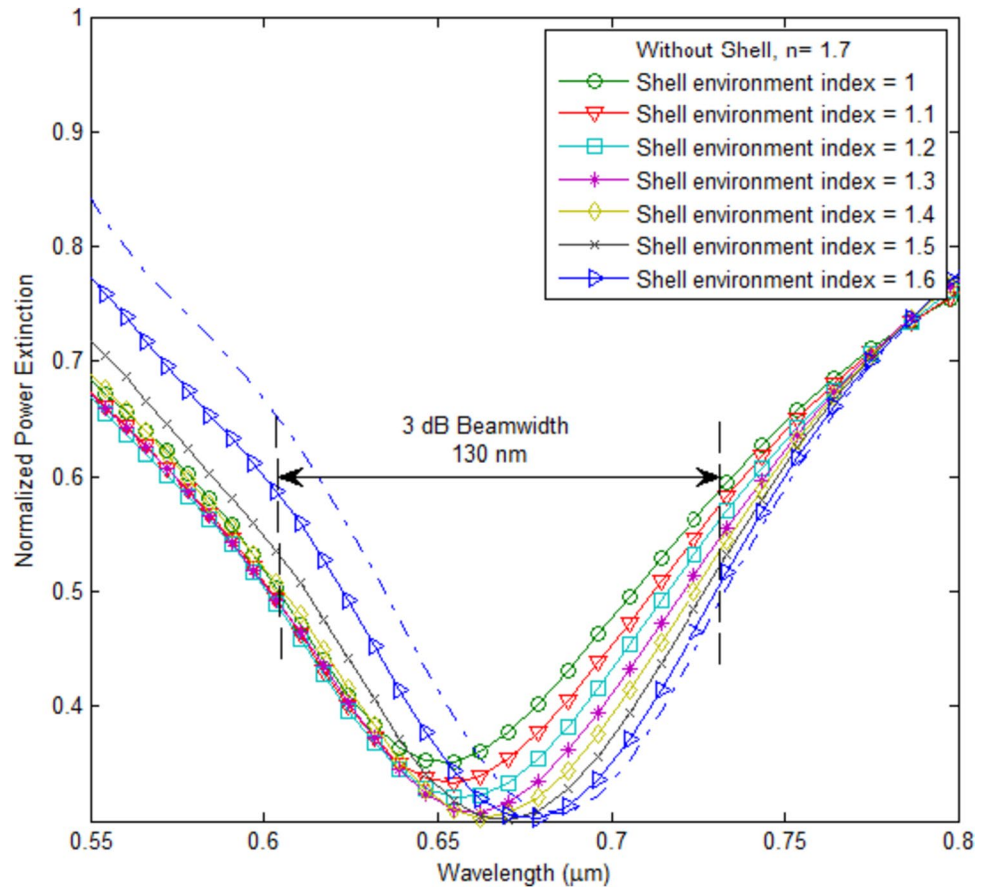
wavelength on the shell refractive index while implementing the first type of array design. One more important observation from the power extinction behaviors of the designs is that the significant red shift in the power extinction resonance is observed for higher surrounding host index values. In all the three discussed shell index cases, the shift starts to appear for surrounding index value 1.3 and it becomes more and more significant with higher surrounding index values. This is the reason why the power extinction peak to peak resonance wavelengths shift and consequently the 3-dB bandwidth is lowest for shell index 1.5 and highest for shell index 1.95 (see Table 1). This observation is also

in agreement with the results shown in Fig. 4b and e where the extinction resonance wavelength increases rapidly as the index contrast value falls below 1.5. This index contrast threshold of 1.5 corresponds to a surrounding index value of 1.3 for a shell index of 1.95.

Now based on the previous discussion, we can clearly differentiate the requirements of the two proposed design structures working as filter and antenna simultaneously. Since different shell index offers different wavelength range of operation hence they can be selected based on the required wavelength range of operation. Further the 3-dB bandwidth of the filter can be controlled by controlling the variation of surrounding index of the dielectric shell. Lower surrounding index values ($N_{env} \leq 1.3$) offer lower filter bandwidth, whereas increasing the surrounding index values will give rise to the increment in filter bandwidth. Using this approach a filter can be designed by gradually varying the host index (graded index variation of refraction) and using the identical dielectric shells in an array offering the required 3-dB bandwidth in accordance with the range of the surrounding index (N_{env}) variation. It is to be noted here that different shell index offer distinct resonance wavelength but they may overlap in their 3-dB bandwidth spectrum. Similar to the power extinction behavior, the radiation characteristics varies in its resonance wavelength and radiation 3-dB band width with dielectric shell index and host index variation, respectively. Red shifting the radiation pattern requires increment in the shell index while the radiation spectrum bandwidth can be controlled by controlling the range of dielectric host index variation.

Again from Table 1, a shift of 40 nm in the start of the filtering operation (filter 3 dB range) can clearly be observed with shell index increment of 0.2 units and the shift increases to 50 nm in case of 0.25 units of shell index increment. Hence red shifting of the spectrum is directly proportional to the values of shell refractive index present in the array. This gives us one more way to alter the desired bandwidth of filter operation and this is also the concept of second filter design. A wider separation between the lowest and the highest shell index values will provide wider 3-dB filter bandwidth and a wider radiation spectrum. With this approach, the two different filtering wavelength ranges present in Table 1 can be combined to achieve a wider wavelength range of operation. In this paper, simulation results for both the types of array design have been presented and analyzed for their application in filter and antenna design. It is to be noted here that more combinations of array design can also be investigated to further match the requirement of filtering operation. For example, the second type of array design has been discussed with keeping the surrounding

Fig. 9 Power extinction (filter operation) by metal nanoparticle in a dielectric shell of index 1.7



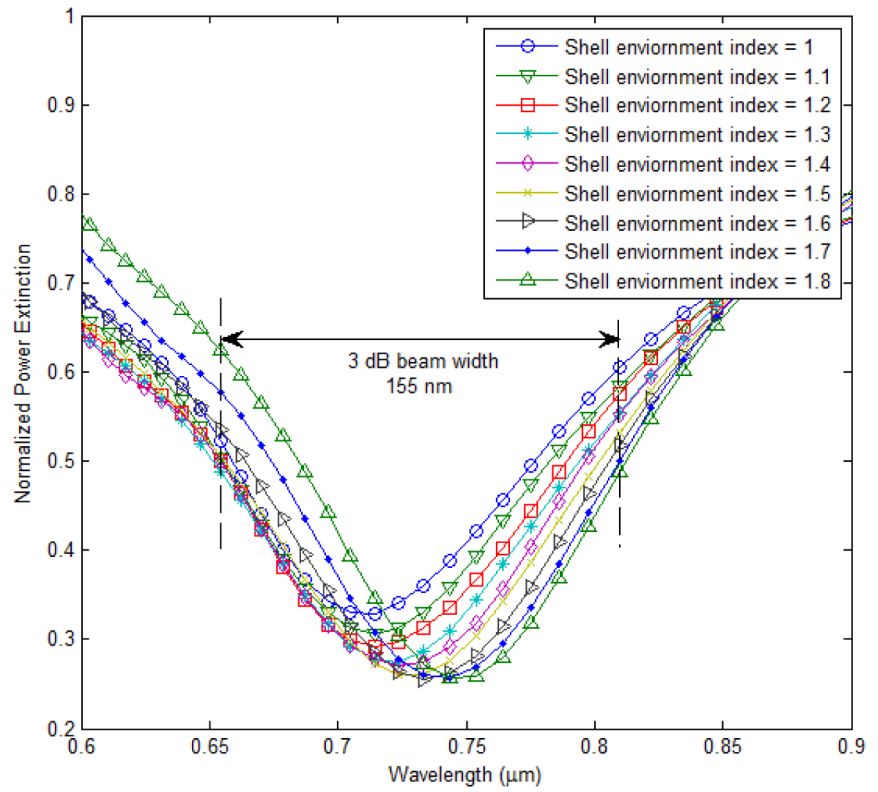
index constant whereas varying the shell index only but here different surrounding index for each element of the array can be used providing different index contrast and consequently altering the overall filter bandwidth and radiation spectrum.

Figure 11 is showing the implementation of the first type of array where surrounding index varies throughout the array and shell index is kept constant. There are 5 elements in the array in a uniformly distributed surrounding index profile increasing from corner to centre. Highest index in the centre of the array provide minimum losses of the excitation field and maximum confinement within the host material. Figure 12 is showing the extinction (Fig. 12a) and radiation (Fig. 12b) responses of the array along with the individual responses of array elements. Here, the surrounding index (N_{env}) variation is considered to be on the higher side ($N_{env} > 1.3$) offering wider bandwidth both in filter and antenna operations. Moreover, considering the minimum number of dielectric shell elements required introducing the effect of three different surrounding conditions results in a 3 element array. This array although breaks the symmetry achieved by the 5 element array but offers the same power extinction behavior as can be seen through Fig. 12c. The

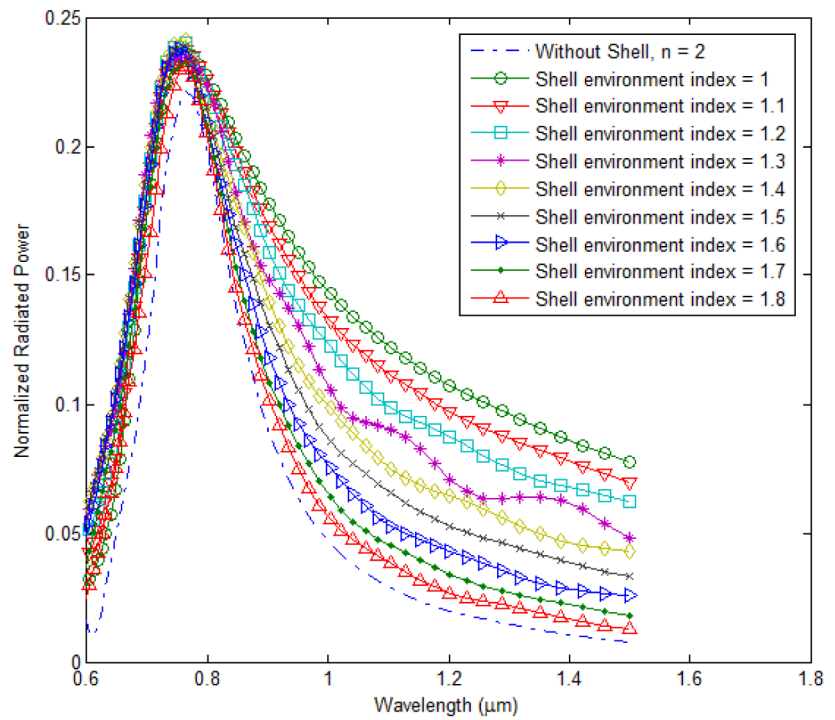
array with 3 elements also has the highest surrounding index at the centre and the lower ones at both the corners. Hence the filter operation offered by the array is purely depending upon the unique combination of dielectric shell and its environment.

Now, commenting on the field pattern offered by the proposed design shown in Fig. 11 and its 3 element variant discussed just in the previous section. Figure 13 shows the near-field and far-field patterns for the aforementioned designs. The change in the number of array elements manifests in terms of the change in the offered far field distribution and hence the radiation pattern offered by a 5 element array is more elliptical than that of a 3 element array (see Fig. 13a and b). Hence increasing the number of elements in the array makes the radiation pattern more directive in one direction by narrowing the beamwidth. This gives an idea about how the main beam shape can be controlled while the nanodielectric shell array is operating as an antenna. Moreover, in order to control polarization mode dispersion, nanoantenna can also be designed for coupling with highly birefringent fibers or waveguides [30, 31]. Figure 13c and d is showing the near-field distribution

Fig. 10 Power extinction (filter operation) **(a)** and radiation **(b)** by the metal nanoparticle in a shell of index = 1.95



(a)



(b)

Table 1 Effect of dielectric shell index variation on filtering operation. (λ_l) is lower 3-dB cut off wavelength and λ_h higher 3-dB cut off wavelength

S.No	Shell index	Peak to peak resonance shift (nm)	Filter resonance range (μm)	Filter 3-dB bandwidth (nm)	3-dB range (μm) ($\lambda_l - \lambda_h$)
1	1.5	20	0.597–0.617	87	0.563–0.65
2	1.7	33	0.654–0.687	130	0.60–0.73
3	1.95	40	0.714–0.754	155	0.6543–0.8097

for the dielectric shell array with 5 elements and 3 elements, respectively. The localized field generated at the gold-dielectric interface appears at the surface of dielectric shell and get coupled with the scattered field of dielectric shell. In addition, since the centre of the array has highest surrounding index, the generated localized field at metal-dielectric and at dielectric-dielectric interface get accumulated at the centre of the array. The distribution of the field is uniform for 5 element array as it has a uniform surrounding index distribution with respect to the centre, whereas in case of 3 element array the field distribution is non-uniform due to nonuniform index distribution. From Fig. 13d, weaker confinement of the field toward $N_{env}=1.6$ is observed in comparison to other side with index $N_{env}=1.7$.

Figure 14 shows the 3D refractive index profile of the second type of the proposed array design offering filter and antenna operations. As discussed previously, the design combines the operational bandwidths of different dielectric shell indices considered in the array while keeping the surrounding index constant. The design has been simulated for four different values of shell indices $N_{shell} = 1.82, 1.89, 1.95,$ and 1.73 . The surrounding index has a constant value of 1.5. It is to be noted here that for effective confinement of the incident light, the placement of the shells is such that the

highest index shell remains at the centre and shell index decreases as we move away from the centre.

Table 2 is showing a comparison of 3 dB filter spectrum offered by the lowest ($N_{shell} = 1.73$) and highest ($N_{shell} = 1.95$) indexed dielectric shells present in the array of the second design along with that of the array itself. It can be clearly seen that the array shown in Fig. 14 offers the response which includes the responses of highest and lowest index dielectric shell. Moreover, the power extinction and radiation responses offered by the array are shown in Fig. 15a and b, respectively. Array offers a 3-dB filtering range of 210 nm which starts at 600 nm and ends at 810 nm including the operational range of the lowest and highest index shell. Likewise, the amplitude of the power extinction response also increases with respect to the individual element response including radiation characteristics of individual elements. Hence, it is possible to combine the individual responses of the dielectric shell elements and to have a collective filtering and radiation characteristics as per the required application.

Finally, the observed electric field pattern of the surface plasmon at the gold-dielectric interface, at the surface of the dielectric shell, and the far field pattern for the design in Fig. 14 are shown in Fig. 16a, b, and c, respectively. When the resonance condition is met, localized field enhancement

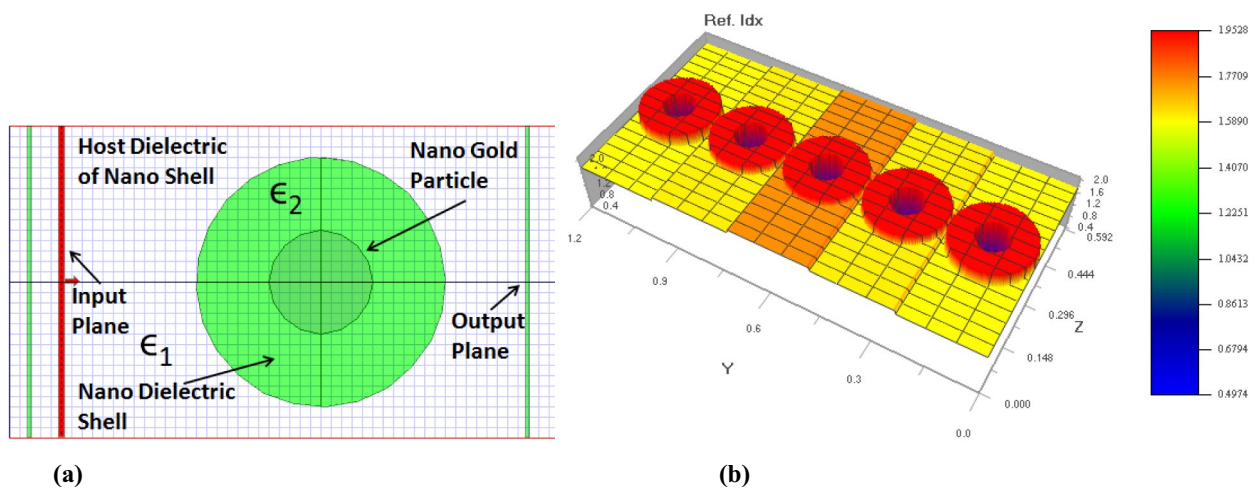
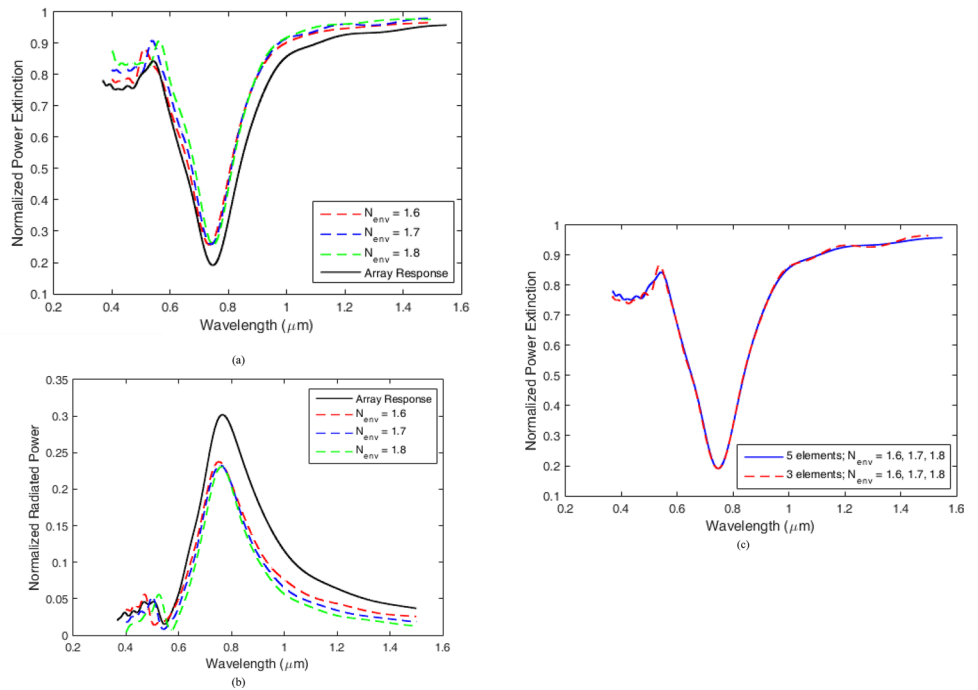


Fig. 11 Side view of the design layout in opti-FDTD **a**; 3-D view of refractive index profile of the first type of proposed nanoparticle array of 5 dielectric shells **(b)**. N_{env} varies from 1.6 to 1.8, and the shell

index is 1.95; the surrounding index profile increases from corner to centre uniformly

Fig. 12 Power extinction (a), and Radiated power (scattering response) (b) for the proposed array shown in Fig. 11. Comparison between the power extinction responses of a 3 element and a 5 element array with identical surrounding index (N_{env}) conditions (c)



at the surface of gold nanoparticle is causing the generation of electric dipole modes which propagates to the surface of dielectric shell and get coupled with the electric dipole

modes of the dielectric shell, as discussed in the paper previously. Now Fig. 16 is clearly showing the generation of plasmon dipole (Fig. 16a), and the resonances at the surface

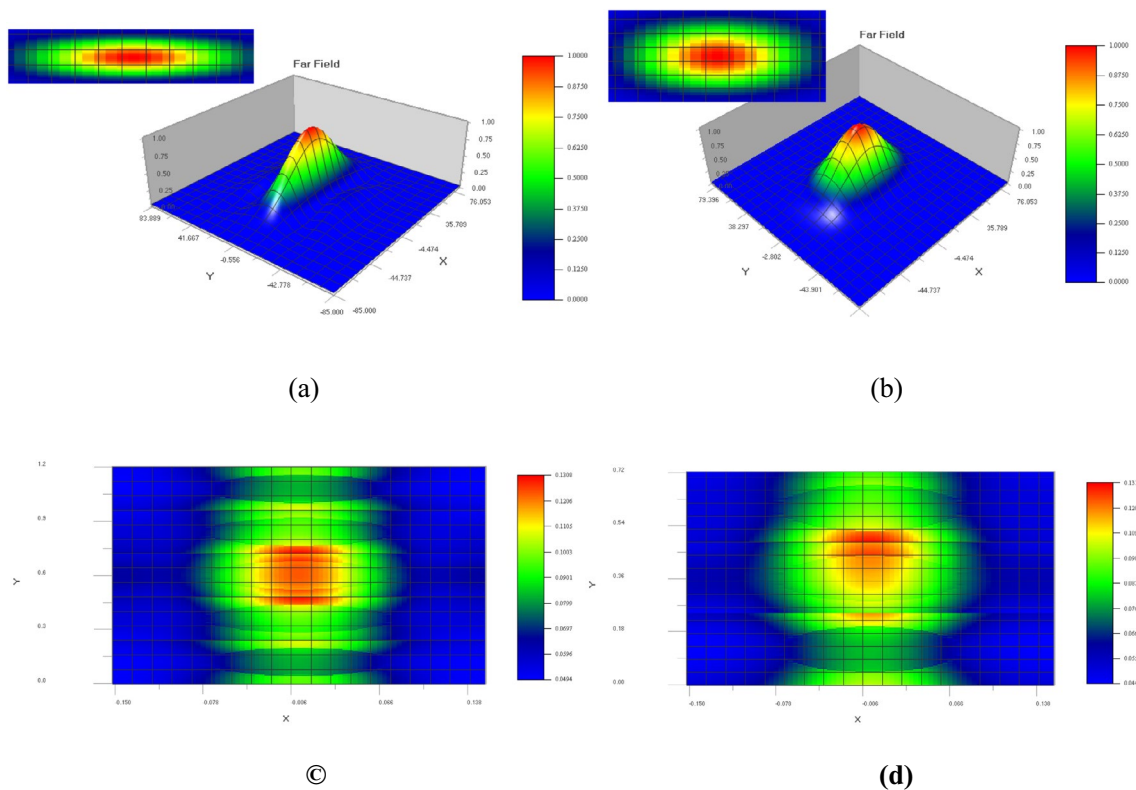


Fig. 13 Far field radiation pattern offered by (a) the 5 element array shown in Fig. 11 a; (b) the 3 element array with similar shell index and surrounding index conditions. Near-field distribution for (c) 5 element array; (d) 3 element array

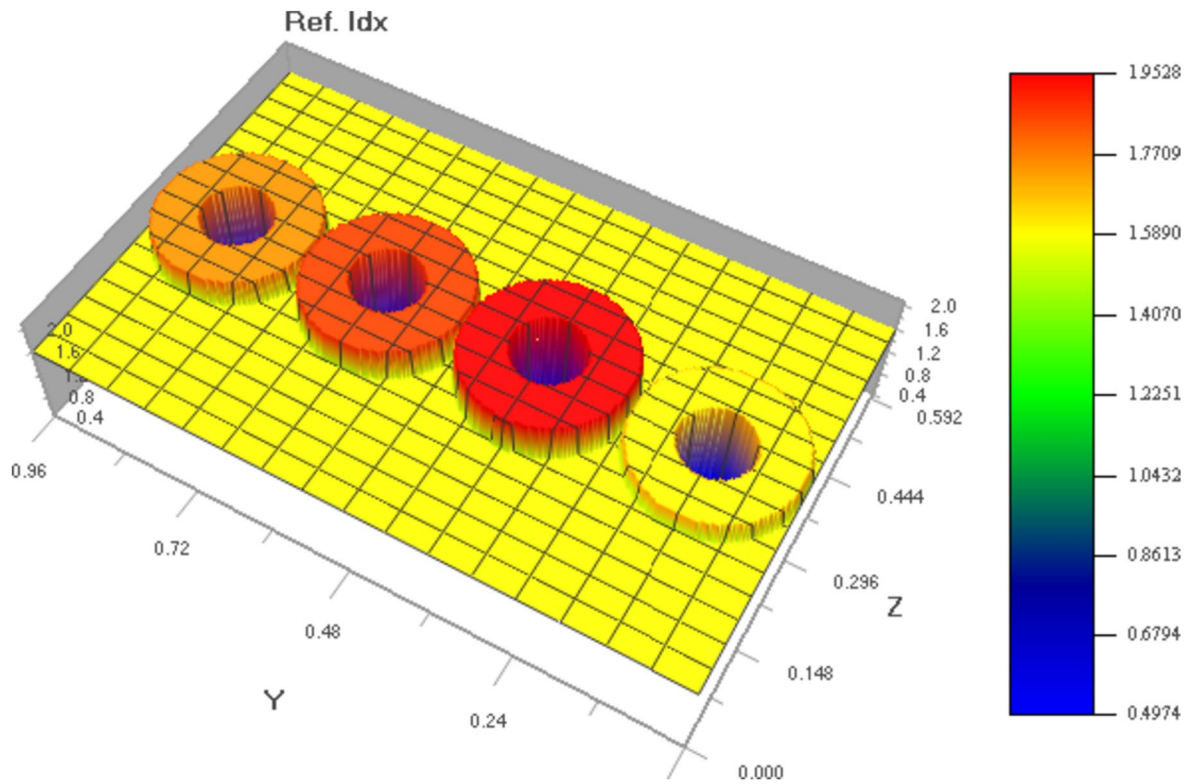


Fig. 14 3D view of the refractive index profile of the second type of array design with different dielectric shell indices. N_{shell} from left to right 1.82, 1.89, 1.95, 1.73, respectively

Table 2 Filter bandwidth with shell index variation and constant environment index $N_{env}=1.5$

S.No	Shell index	Filter 3-dB bandwidth (nm)	3-dB range (μm) ($\lambda_l - \lambda_h$)
1	1.72	118	0.61–0.728
2	1.95	150	0.65–0.80
3	Array (Fig. 14)	210	0.60–0.81

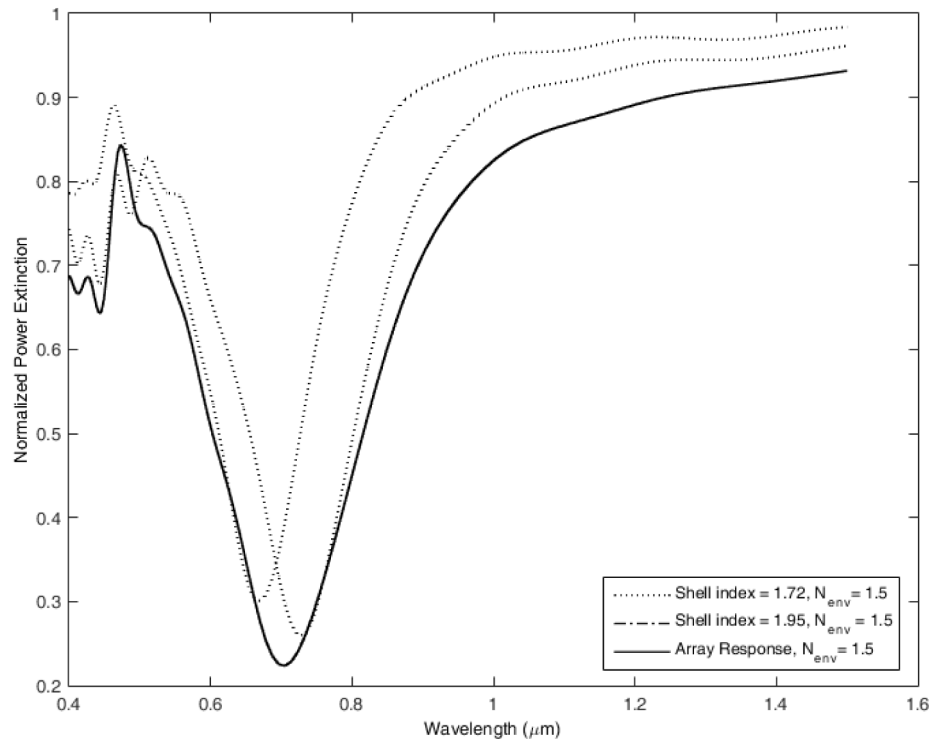
of dielectric shells which is producing the localized hotspots between the shells, and relatively lighter intensities at the corner shells on the outer side (see Fig. 16b). From Fig. 16c, it should be noted that the radiation pattern generated by the array offers a main beam which is less elliptical than 5 element array whereas slightly more elliptical than a 3 element array (see Fig. 13). This gives a clear idea about controlling the pattern with number of elements in the array.

Conclusion

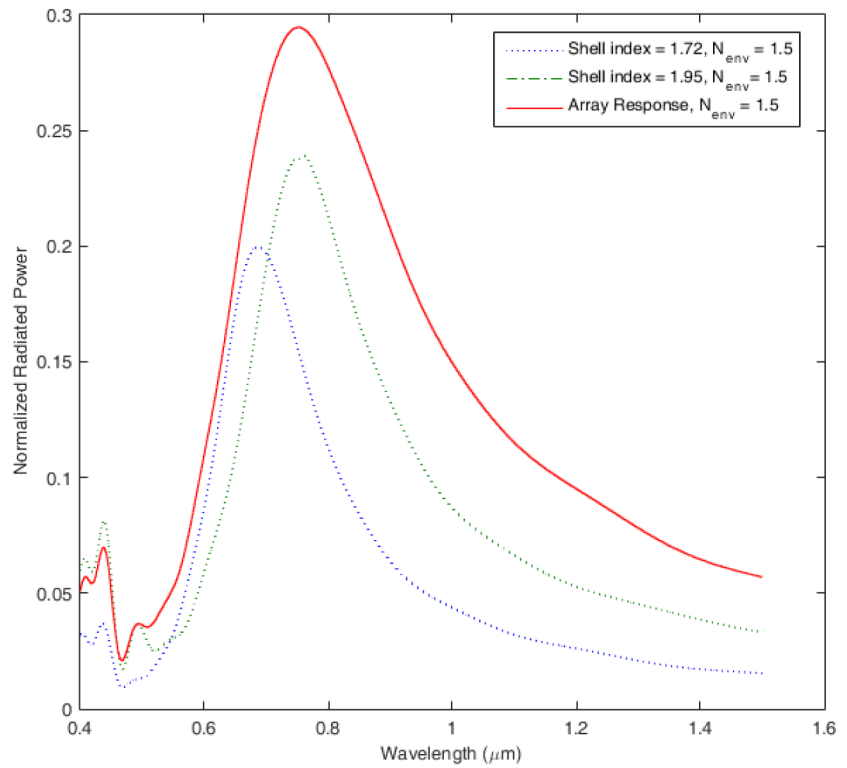
In this paper, a hybrid nanostructure having gold nanoparticle embedded in a 2.4 times larger dielectric shell has been investigated for its filtering and radiative characteristics

when placed in an array. The structure has been optimized in its dimensions with an objective of getting gold nanoparticle characteristics similar to the infinite surrounding environment. The proposed structure offers power extinction and radiation characteristics as a result of dominating electric field resonances in metal and magnetic field resonances in dielectric shell. Weak coupling between electric fields resonances of metal and dielectric causes approximately no change in the gold nanoparticle scattering resonance wavelength, whereas total power extinction resonance wavelength changes due the presence of dominating magnetic dipole mode of dielectric shell. The structure offers a maximum power extinction resonance shift of 40 nm corresponding to a maximum 3 dB filter bandwidth of 155 nm for shell index 1.95, when changing the shell environment index. Similarly, shell indices 1.5 and 1.7 offer a 3 dB filter bandwidth of 87 nm, 130 nm, respectively. Further, wider filter bandwidths were achieved in the second type of array design when shell indices from 1.73 to 1.95 were placed in an environment of constant index. The array offered a wide filtration width of 210 nm. On the other end, scattering characteristics offered by the array of hybrid structure remains almost invariable in terms of resonance wavelength with change in the shell environment index but it had a wider 3 dB spectral width with increased amplitude.

Fig. 15 Two element array filter design with shell indices = 1.7, 1.95; host index = 1.5; Extinction response of the array (a); Radiation response of the array (b); the metal particle is identical in both the shells

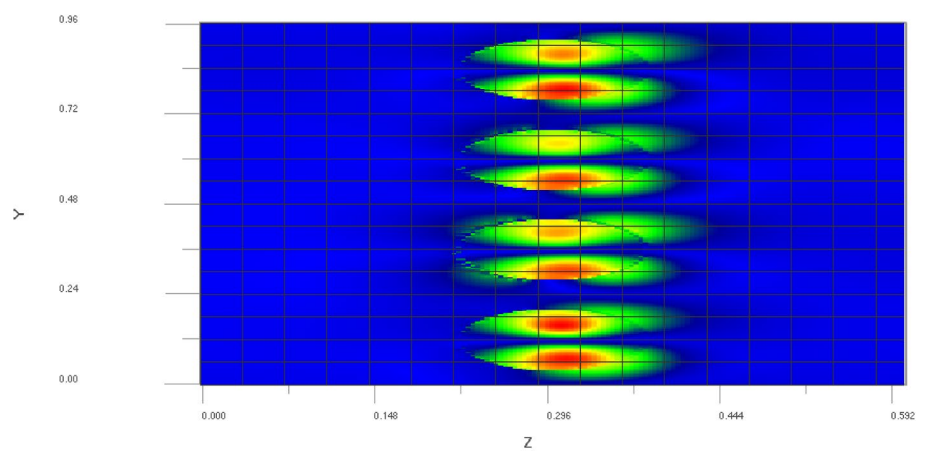


(a)

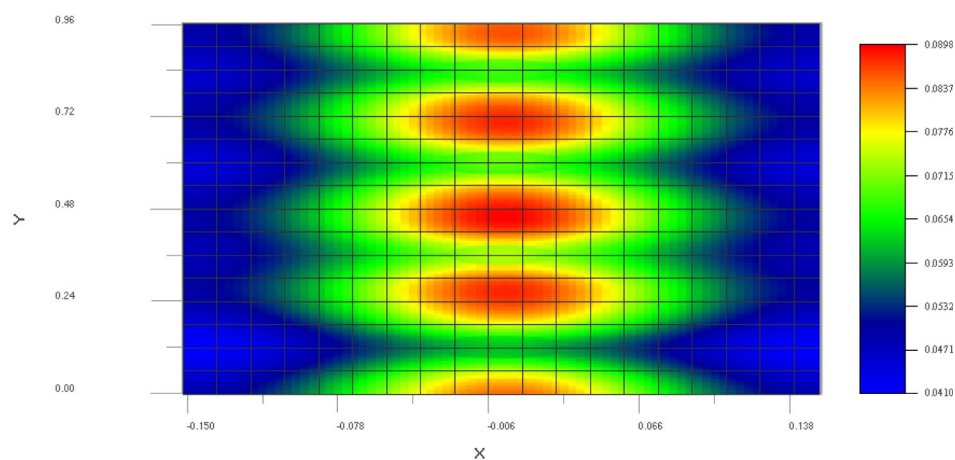


(b)

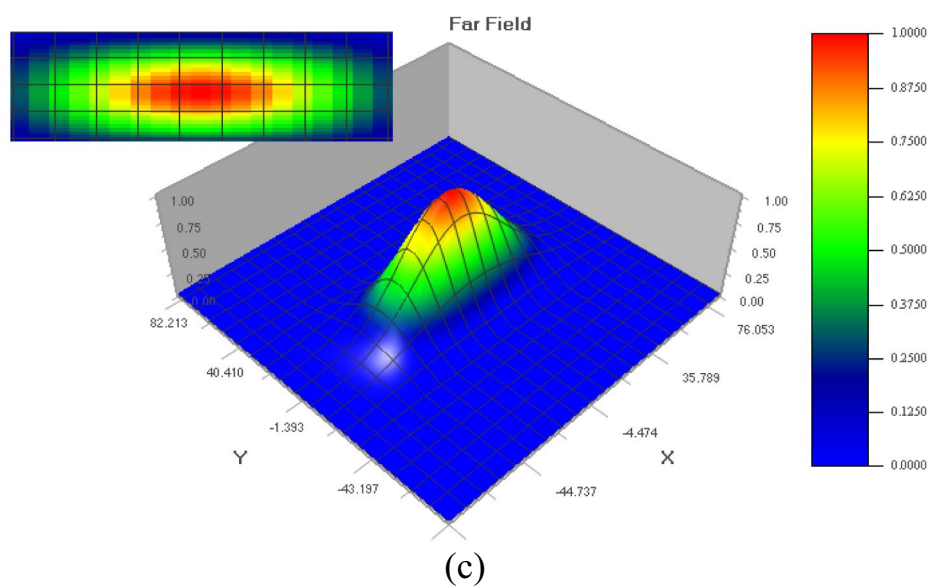
Fig. 16 **a** Surface plasmon electric dipole mode generation, **b** electric field resonance at the surface of dielectric nanoshells with hot spot between the shells, **c** far field radiation pattern



(a)



(b)



(c)

In addition, array having dielectric shells of different indices in an environment of constant index offers a very wide spectrum of radiation as it includes number of resonance wavelengths. It was also observed that by only changing the number of elements do not have any impact on power extinction and radiation characteristics of the array, whereas it alters the far field radiation pattern by changing the main beam shape.

Acknowledgements The authors would like to acknowledge support provided by DST (Department of Science & Technology), New Delhi [Indo-Poland Joint research grant: DST/INT/POL/P-51/2020].

Author contributions VK As a first author, developed the concept, finalize the tool for simulation, simulate the design, and draft the manuscript. RZ has contributed in performing the formal analysis of the simulation result, verification of the data from the literature survey and drafting the manuscript. PKJ has assisted for obtaining the result with the aid of software. He also reviewed and edited the manuscript. VJ has contributed in analysis of simulation work. He has also handled the review and final editing of the manuscript.

Funding No funding.

Data availability The manuscript does not contain any third party material.

Declarations

Conflict of interests Authors declare that they have no known competing financial interests or personal relationships that could have appeared to influence the work.

References

1. D.W. Pohl in *Near-Field Optics, Principles and Applications*, edited by X. Zhu and M. Ohtsu (World Scientific, Singapore, 2000), pp. 9–21.
2. L. Novotny, Effective wavelength scaling for optical antennas. *Phys. Rev. Lett.* **98**, 266802 (2007)
3. J. Wessel, Surface-enhanced optical microscopy. *J. Opt. Soc. Am. B* **2**, 1538–1541 (1985)
4. L. Novotny, S.J. Stranick, Near-field optical microscopy and spectroscopy with pointed probes. *Annu. Rev. Phys. Chem.* **57**, 303–331 (2006)
5. J.N. Farahani, D.W. Pohl, H.-J. Eisler, B. Hecht, Single quantum dot coupled to a scanning optical antenna: a tunable superemitter. *Phys. Rev. Lett.* **95**(1), 017402 (2005)
6. T.H. Taminiau, F.B. Segerink, R.J. Moerland, L. Kobus Kuipers, N.F. van Hulst, Near-field driving of a optical monopole antenna. *J. Opt. A Pure Appl. Opt.* **9**(9), S315 (2007)
7. S.S. Kharintsev, G.G. Hoffmann, A.I. Fishman, M. Kh Salakhov, Plasmonic optical antenna design for performing tip-enhanced Raman spectroscopy and microscopy. *J. Phys. D Appl. Phys.* **46**(14), 145501 (2013)
8. H.M. Rabiul, O.G. Hellesø, Dielectric optical nanoantennas. *Nanotechnology* **32**(20), 202001 (2021)
9. J. Schuller, E. Barnard, W. Cai et al., Plasmonics for extreme light concentration and manipulation. *Nat. Mater.* **9**, 193–204 (2010)
10. C. Höppener, L. Novotny, Antenna-based optical imaging of single Ca²⁺ transmembrane proteins in liquids. *Nano Lett.* **8**, 642–646 (2008)
11. T.S. Van Zanten, M.J. Lopez-Busquets, M.F. Garcia-Parajo, Imaging individual proteins and nanodomains on intact cell membranes with a probe-based optical antenna. *Small* **6**, 270–275 (2010)
12. P. Bharadwaj, B. Deutsch, L. Novotny, Optical antennas. *Adv. Opt. Photon.* **1**(3), 438–483 (2009)
13. P. Mhlschlegel, H.-J. Eisler, O.J.F. Martin, B. Hecht, D.W. Pohl, Resonant optical antennas. *Science* **308**(5728), 1607–1609 (2005)
14. J. Farahani, D. Pohl, H.J. Eisler, B. Hecht, Single quantum dot coupled to a scanning optical antenna: a tunable superemitter. *Phys. Rev. Lett.* **95**, 017402 (2005)
15. K. Crozier, A. Sundaramurthy, G. Kino, C. Quate, Optical antennas: resonators for local field enhancement. *J. Appl. Phys.* **94**(7), 4632–4642 (2003)
16. N. Horiuchi, Integrated optical antenna. *Nat. Photonics* **14**, 134 (2020)
17. Y. Park, J. Kim, Y.G. Roh, Q.H. Park, Optical slot antennas and their applications to photonic devices. *Nanophotonics* **7**(10), 1617–1636 (2018)
18. H. Mertens, A.F. Koenderink, A. Polman, Plasmon-enhanced luminescence near noble-metal nanospheres: comparison of exact theory and an improved Gersten and Nitzan model. *Phys. Rev. B* **76**, 115123 (2007)
19. A.F. Koenderink, On the use of Purcell factors for plasmon antennas. *Opt. Lett.* **35**, 4208–4210 (2010)
20. J.J. Greffet, M. Laroche, F. Marquier, Impedance of a nano antenna and a single quantum emitter. *Phys. Rev. Lett.* **105**(11), 117701 (2010)
21. V. Kanungo, Design and Synthesis of Planar Antenna Array in RF Domain using GA Modified Discretizing Technique of Taylor distribution and Analysis of Nanoparticle Arrays for Optical Antenna and Filter Design, PhD thesis, Malaviya National Institute of Technology (2017)
22. S.A. Maier, *Plasmonics: fundamentals and applications* (2007)
23. X. Ou, Y. Liu, M. Zhang, Li. Hua, S. Zhan, Plasmonic gold nanostructures for biosensing and bioimaging. *Microchim. Acta* **188**(9), 304 (2021)
24. M. Omrani, R. Keshavarzi, M. Abdi-Jalebi et al., Impacts of plasmonic nanoparticles incorporation and interface energy alignment for highly efficient carbon-based perovskite solar cells. *Sci. Rep.* **12**, 5367 (2022)
25. M. Righini, P. Ghenuche, S. Cherukulappurath, V. Myroshnychenko, F.J. Garcia de Abajo, R. Quidant, Nano-optical trapping of Rayleigh particles and Escherichia coli bacteria with resonant optical antennas. *Nano Lett.* **9**, 3387–3391 (2009)
26. J. Li, Z. Zhu, B. Zhu, Y. Ma, B. Lin, R. Liu, Y. Song, H. Lin, Tu. Song, C. Yang, Surface-enhanced Raman scattering active plasmonic nanoparticles with ultrasmall interior nanogap for multiplex quantitative detection and cancer cell imaging. *Anal. Chem.* **88**(15), 7828–7836 (2016)
27. V. Amendola, R. Pilot, M. Frascioni, O.M. Maragò, M.A. Iatì, Surface plasmon resonance in gold nanoparticles: a review. *J. Phys. Condens. Matter* **29**(20), 203002 (2017)
28. C.Z. Tan, Determination of refractive index of silica glass for infrared wavelengths by IR spectroscopy. *J. Non-Cryst. Solids* **223**, 158–163 (1998)
29. A.I. Kuznetsov, A.E. Miroshnichenko, M.L. Brongersma, Y.S. Kivshar, B. Luk'yanchuk, Optically resonant dielectric nanostructures. *Science* **354**(6314), aag2472 (2016)
30. N.N. Li, Y.H. Lai, S.H. Lam, H.Y. Bai, L. Shao, J.F. Wang, Directional control of light with nanoantennas. *Adv. Optical Mater.* **9**, 2001081 (2021)

-
31. F.J. González, J. Alda, Optical nanoantennas coupled to photonic crystal cavities and waveguides for near-field sensing. *IEEE J. Sel. Top. Quantum Electron.* **16**(2), 446–449 (2010). <https://doi.org/10.1109/JSTQE.2009.2027444>

Springer Nature or its licensor (e.g. a society or other partner) holds exclusive rights to this article under a publishing agreement with the author(s) or other rightsholder(s); author self-archiving of the accepted manuscript version of this article is solely governed by the terms of such publishing agreement and applicable law.

Publisher's Note Springer Nature remains neutral with regard to jurisdictional claims in published maps and institutional affiliations.